Universal version of density-functional theory for polymers with complex architecture

Xiaofei Xu, Dapeng Cao,* Xianren Zhang, and Wenchuan Wang
Division of Molecular and Materials Simulation, Key Laboratory for Nanomaterials Ministry of Education, Beijing University of Chemical Technology, Beijing 100029, People's Republic of China
(Received 26 August 2008; revised manuscript received 11 December 2008; published 26 February 2009)

We propose a density-functional theory for inhomogeneous polyatomic fluids with complex architecture by introducing a different representation for the polymers. This representation gives an efficient hierarchical algorithm to calculate the direct bonding connectivity integral for polymers with complex architecture, such as linear, star, branched, and dendritic structures. A comparison with the available simulated data for linear and star polymers confirms the accuracy of the present theory in reproducing the density profiles of the two types of polymer in the slits. By using the proposed algorithm, we also explore partitioning coefficients of polymers of different architectures in a slit, and find that the partitioning coefficients of branched, star, and dendrimer forms of 22-mers decrease to a minimum at extremely low packing fraction, and then increase monotonically with packing fraction. Moreover, it is found that it is more difficult for a linear polymer of 22-mers to enter the slit than for branched, star, and dendritic polymers. In addition, we also investigate the self-assembly of diblock copolymers with different tails in a slit. It is found that the linear copolymer self-assembles into a trilayer film structure, while copolymers with branched and dendritic tails self-assemble into a five-layer film structure. Interestingly, the copolymer with a star tail self-assembles into a trilayer film structure, and then the trilayer structure evolves into a five-layer structure with increase of the bulk packing fraction in the case studied.

DOI: 10.1103/PhysRevE.79.021805 PACS number(s): 36.20.−r, 68.47.Mn

I. INTRODUCTION

Density-functional theory (DFT) of polyatomic fluids, pioneered by Chandler, McCoy, and Singer [1] (CMS), has been proved to be a versatile and powerful tool to investigate the microstructure and thermodynamic properties of polymers under a variety of situations. The original theory of CMS is a generalization of monatomic DFT to polyatomic fluids, in which all intramolecular correlations were included in the ideal free energy and the intermolecular interactions in the excess part. In the CMS DFT the free energy is expressed as a functional of the single-site densities, not as a functional of the polymeric molecular distribution. Kierlik and Rosinberg [2] reported a perturbation-based DFT in which the ideal free energy is expressed as a functional of the full molecular density distribution, and the excess contribution is calculated perturbationally over a reference fluid of monomers at the same temperature and density. Qualitative agreement with simulated data was found for short chains at high densities, but the theory failed for long chains and low densities because of the neglect of the intramolecular excluded volume effect. Woodward and Yethiraj [3] improved the functional by adopting the generalized Flory-Dimer (GFD) equation of state (EOS), which has been shown to be very accurate in comparison with simulated results. The GFD equation supersedes the original generalized Flory theory by using an empirical EOS for dimers to estimate the probability of inserting bonded pair monomers [4].

By considering the intramolecular excluded volume effect and the relationship between the weighted functions and the geometrical properties of a sphere, Rosenfeld [5] developed a well-known weighted DFT for hard-sphere fluids, i.e., fundamental measure theory (FMT). It was first proposed for single-site hard spheres, and was later introduced to polymeric DFTs by incorporating a bonding contribution to the free energy. Although the FMT met with considerable success, it is slightly inaccurate in predicting coexisting fluids and overestimates the pressure of pure hard-sphere fluids at densities approaching bulk freezing [6]. The reason for these inaccuracies may be that the underlying EOS of bulk fluids in FMT is from the Percus-Yevick (PY) equation. Therefore, Roth *et al.* [6] and Yu *et al.* [7] modified the FMT theory separately by using the empirical Mansoori-Carnahan-Starling-Leland EOS to replace the PY EOS [8]. The modified FMT- (MFMT-)based DFT [6,7], has been successfully applied to investigating adsorption and surface phase transitions [9–11], the microstructure of flexible polymer fluids [12–14], surface forces between polymer brushes [15,16], and osmotic pressure of caged DNA in the bulk [17]. Moreover, it was also extended to investigations of inhomogeneous semiflexible and cyclic polyatomic fluids [18], grafted polyelectrolytes [19], and rodlike molecules [20,21]. All these calculations suggest that the MFMT-based DFT can excellently reproduce the microstructure and thermodynamic properties of polymeric fluids. However, the MFMT-based DFT has difficulty in predicting the thermodynamic properties of polymers with complex architecture because of the direct bonding integral of the complex architecture. By treating the ideal free energy exactly via a single-chain simulation, single-chain Monte Carlo (SCMC) simulation [22–25] allows us to investigate polymer models that have quite complex intramolecular interaction, such as dendrimers [26]. However, it is not in a self-consistent framework from the theoretical point of view.

In this work, we introduce a different representation for polymers and present a universal version of DFT for systems containing polyatomic molecules with complex architectures, such as linear, branched, star, or dendritic structures.

*FAX: +8610-64427616. caodp@mail.buct.edu.cn; cao_dp@hotmail.com

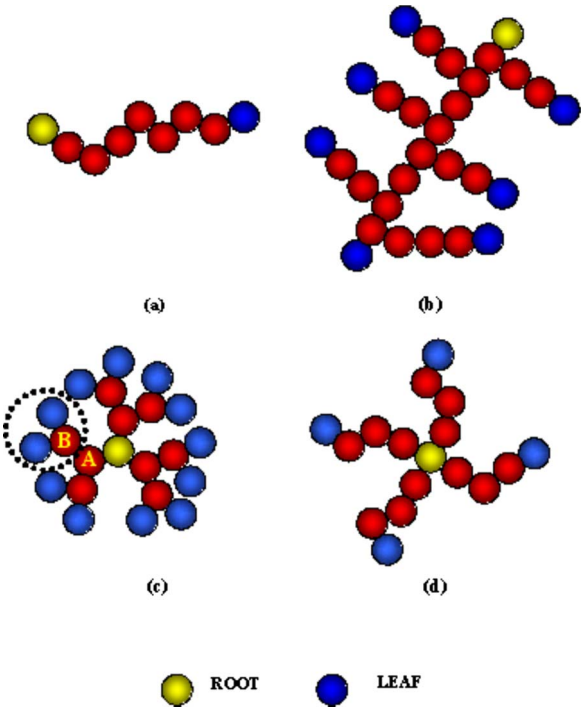

FIG. 1. (Color online) Representation of polymers with complex architecture by tree-type structures: (a) linear, (b) branched, (c) G3 dendrimer, and (d) star polymer.

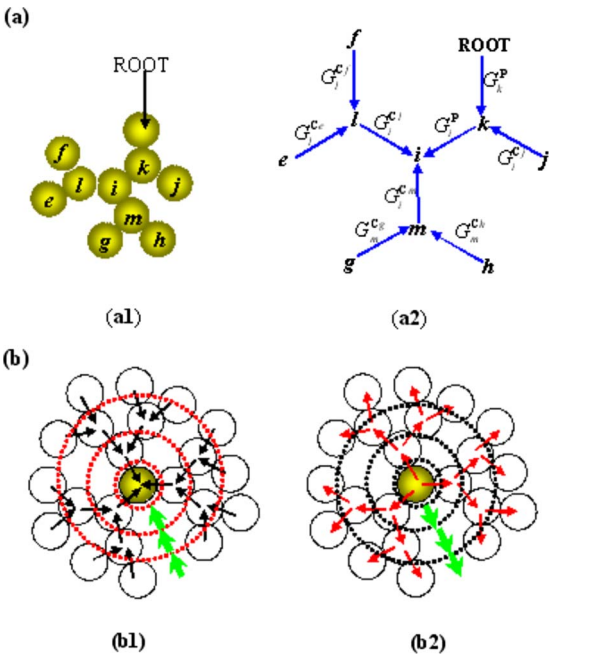

FIG. 2. (Color online) (a) Schematic diagrams for computing the segmental density ρ_{si}, using a dendritic polymer as an example. (a1) Dendritic polymer. (a2) Flowchart for computing ρ_{si}. (b) The two traverses in calculating recursive functions according to Eqs. (6) and (7). (b1) Searching over parents to calculate all child-recursive functions $G_i^{C\alpha}(z)$ [α=child(i)]. The calculations were carried out from every leaf to the root level by level, which means that we must calculate all the bonding connectivities at maximum level L first, and then calculate these at levels $L-1$, $L-2$,…, up to level 1. (b2) Searching over children to calculate all parent-recursive functions $G_i^{P}(z)$. The calculations were carried out from the root to every leaf level by level.

II. MODELING, THEORY, AND ALGORITHM

A. Modeling

A coarse-grained model is used to represent the polymers with complex architecture, where the bonding length between two neighboring segments is fixed as the segmental diameter σ and the bonding angle is fully flexible. We use the tree-type structure in graph theory to represent a polymer. As shown in Fig. 1, all the polymers with different architectures (including linear, branched, star, and dendritic structures) can be modeled by a tree-type structure. In the model, we must first assign a segment (no special requirement on this segment) as the *root*. Then, a polymer can be considered exactly as a tree-type structure. The part connected to the root is defined as a subtree, where the connected segment is identified as the root of the subtree. The root of the subtree is called a *child* of the root segment, and the root segment is accordingly called the *parent* of the child. For example, the dashed line in Fig. 1(c) is a subtree of segment A. The connected segment B is the root of the subtree. Segment B is a child of segment A, and segment A therefore is the parent of segment B. A segment is a *leaf* if there is no child for this segment. For example, all segments e, f, g, h, j are leaves of the tree in Fig. 2(a1). A segment is at *level* L if the parent-child relation transfers L times between this segment and the root. For instance, the level of segment A in Fig. 1(c) is 1, as segment A is a child of the root. The parent-child relation transfers twice between segment B and the root, as B is a child of A and A is a child of the root. Therefore, the level for segment B is 2. For consistency, we define the level of the root as zero. For a polymer containing N segments, we use unique integer series from 1 to N to distinguish and index each segment. There is no special requirement on this index.

B. Density-functional theory

Let us recall the framework of density-functional theory briefly before presenting the universal version for polymers with complex architecture. For a polymeric fluid, the grand potential is related to the Helmholtz energy functional via Legendre transformation

$$\Omega[\rho_{\mathrm{M}}(\boldsymbol{R})] = F[\rho_{\mathrm{M}}(\boldsymbol{R})] + \int d\boldsymbol{R}\ \rho_{\mathrm{M}}(\boldsymbol{R})[\psi_{\mathrm{M}}(\boldsymbol{R}) - \mu_{\mathrm{M}}], \quad (1)$$

where $\rho_{\mathrm{M}}(\boldsymbol{R})$ is a multidimensional density profile, and $\boldsymbol{R}$ is a composite vector $(\boldsymbol{r}_1, \boldsymbol{r}_2, \ldots, \boldsymbol{r}_N)$ representing the positions of all segments of the polymeric molecule. $\psi_{\mathrm{M}}(\boldsymbol{R})$ is the sum of the external potentials exerted on each individual segment, and μ_{M} is the chemical potential of the polymer chain. The molecular density profile $\rho_{\mathrm{M}}(\boldsymbol{R})$ is related to the segmental densities by

$$\rho_{\mathrm{s}}(\boldsymbol{r}) = \sum_{i=1}^{N} \rho_{\mathrm{s}i}(\boldsymbol{r}) = \sum_{i=1}^{N} \int d\boldsymbol{R}\ \delta(\boldsymbol{r} - \boldsymbol{r}_i)\rho_{\mathrm{M}}(\boldsymbol{R}), \quad (2)$$

where $\rho_s(\boldsymbol{r})$ is the total segmental density and $\rho_{si}(\boldsymbol{r})$ is the local density of segment i. The Helmholtz energy functional $F[\rho_M(\boldsymbol{R})]$ is conventionally expressed as an ideal contribution from a system of ideal chains that interact only through bonding potentials and an excess part taking into account the contributions from nonbonded chain connectivity interaction and the hard-sphere repulsion effect. Following our previous work for polymers [14,19], the hard-sphere part of the excess Helmholtz energy functional is represented by a modified fundamental measure theory, and the excess Helmholtz energy functional due to the chain connectivity is given by a generalized first-order thermodynamics perturbation theory (TPT1) [7].

Minimization of the grand potential with respect to the density profiles yields the Euler-Lagrange equations

$$\rho_M(\boldsymbol{R}) = \exp\left(\beta\mu_M - \beta V_B(R) - \beta\sum_{i=1}^{N}\lambda_i(\boldsymbol{r}_i)\right), \tag{3}$$

where the self-consistent potential $\lambda_i(r_i)$ is a summation of the derivatives of the excess Helmholtz energy with respect to the density profiles and the external potential, i.e., $\lambda_i(\boldsymbol{r}_i) = \ddot{a}F_{ex}/\ddot{a}\rho_s(\boldsymbol{r}_i) + \varphi_i(\boldsymbol{r}_i)$. The direct bonding potential $V_B(\boldsymbol{R})$ satisfies

$$\exp[-\beta V_B(\boldsymbol{R})] = \prod_{\substack{i\leftrightarrow j \\ i<j}} \frac{\delta(|\boldsymbol{r}_i - \boldsymbol{r}_j| - \sigma)}{4\pi\sigma^2}, \tag{4}$$

where $i \leftrightarrow j$ stands for the bond connecting segment i and j. Combining Eqs. (2) and (3), we can get the segmental density of a polymer,

$$\rho_s(\boldsymbol{r}) = \int d\boldsymbol{R}\sum_{i=1}^{N}\delta(\boldsymbol{r}-\boldsymbol{r}_i)\exp\left(\beta\mu_M - \beta V_B(\boldsymbol{R}) - \beta\sum_{j=1}^{N}\lambda_j(\boldsymbol{r}_j)\right). \tag{5}$$

For polymers with complex architecture, like star, branched, and dendritic polymers, the key issue in solving Eq. (5) is how to simplify the complex integral of the direct bonding connectivity $[V_B(\boldsymbol{R})]$. By treating the ideal free energy exactly via a single-chain simulation, a hybrid method combining DFT and single-chain simulation [22–25] allows us to investigate polymer models that have quite complex intramolecular interaction, such as dendrimers [26]. From a theoretical point of view, this hybrid method is not in a self-consistent theoretical framework, as mentioned earlier. In this work, by introducing the polymeric representation as a tree-type structure, we develop an efficient method to solve the integral of Eq. (5), and the DFT approach for polymers with different architectures (including linear, star, branched, and dendritic architectures) can be expressed universally.

C. Algorithm

In the present method, the key point is that we can find one and only one path from the root to the segment of interest, or from the segment of interest to the root. This leads to a clear way to calculate the direct bonding connectivity of a complex architecture. For example, in the calculation of the local density of segment i in Fig. 2(a), the contribution of the direct bonding connectivity to the grand potential from every other segment can be accumulated by a traverse from every leaf to i. The traverse is root$\rightarrow k \rightarrow i$ and from every leaf (segments e,f,g,h,j) to i. In the parent-child relation, the traverse is comprised of the sought child (such as root$\rightarrow k$ and $k \rightarrow i$) and sought parent (such as $f \rightarrow l$ and $m \rightarrow i$). In every child or parent obtained, we need to calculate the accumulated weight [G_i^P, $G_i^{C\alpha}$ as shown in Fig. 2(a2)] due to the direct bonding connectivity. The principle of mathematical derivation is the same as this idea above, because the integral in Eq. (5) can be accumulated by this travel.

Next, we present the DFT for polymers with complex architecture in detail. Equations (1)–(5) can therefore lead to the following expression for the segmental density profiles:

$$\rho_{si}(\boldsymbol{r}) = \exp[\beta\mu_M - \beta\lambda_i(\boldsymbol{r})]G_i^P(\boldsymbol{r})\prod_{\acute{a}=\text{child}(i)} G_i^{C\alpha}(\boldsymbol{r}), \quad 1 \leqslant i \leqslant N. \tag{6}$$

The parent-recursive function $G_i^P(\boldsymbol{r})$ is given by

$$G_{i\,[\text{parent}(i)=k]}^{P}(\boldsymbol{r}) = \begin{cases} 1, & i \text{ is root}, \\ \dfrac{1}{4\pi\sigma^2}\displaystyle\int_{|\boldsymbol{r}'-\boldsymbol{r}|=\sigma} \exp[-\beta\lambda_k(\boldsymbol{r}')]G_k^P(\boldsymbol{r}')\prod_{\substack{\acute{a}=\text{child}(k) \\ \acute{a}\neq i}} G_k^{C\alpha}(\boldsymbol{r}')d\boldsymbol{r}', & i \text{ is not root}. \end{cases} \tag{7}$$

The child-recursive function $G_i^{C\alpha}(z)$ $[\alpha=\text{child}(i)]$ is given by

$$G_{i\,[\alpha=\text{child}(i)]}^{C\alpha}(\boldsymbol{r}) = \begin{cases} \dfrac{1}{4\pi\sigma^2}\displaystyle\int_{|\boldsymbol{r}'-\boldsymbol{r}|=\sigma} \exp[-\beta\lambda_\alpha(\boldsymbol{r}')]\prod_{\beta=\text{child}(\alpha)} G_\alpha^{C\beta}(\boldsymbol{r}')d\boldsymbol{r}', & i \text{ is not a leaf}, \\ 1, & i \text{ is a leaf}. \end{cases} \tag{8}$$

We use the symbols "parent(i)" and "child(i)" to represent the parent and child segments of the segment i, respectively. In the calculation of every segmental density ρ_{si}, it is not necessary to calculate Eqs. (7) and (8) every time, but all $G_i^{\mathrm{P}}(\boldsymbol{r})$ and $G_i^{\mathrm{C}\alpha}(\boldsymbol{r})$ [α=child(i)], $i=1,2,\ldots,N$, can be obtained two traverses described below.

(a) Searching over parents to calculate all child-recursive functions $G_i^{\mathrm{C}\alpha}(\boldsymbol{r})$ [α=child(i)] [see Fig. 2(b1)]. The calculations were carried out from every leaf to the root level by level, which means that we must calculate all the bonding connectivities at maximum level L first, and then calculate these at levels $L-1$, $L-2$,..., up to level 1. This special order is determined via Eq. (8), because the calculations at low levels need the results of higher levels as input. For example, in Fig. 2(a) the maximum level is four, and the calculation procedures are as follows.

(1) Calculate all bonding integrals at level four, i.e., $f \rightarrow l$ ($G_l^{\mathrm{C}f}$), $e \rightarrow l$ ($G_l^{\mathrm{C}e}$), $g \rightarrow m$ ($G_m^{\mathrm{C}g}$), $h \rightarrow m$ ($G_m^{\mathrm{C}h}$).

(2) Use $G_l^{\mathrm{C}f}$, $G_l^{\mathrm{C}e}$, $G_m^{\mathrm{C}g}$, and $G_m^{\mathrm{C}h}$ to calculate all bonding integrals at level three, i.e., $l \rightarrow i$ ($G_i^{\mathrm{C}l}$), $m \rightarrow i$ ($G_i^{\mathrm{C}m}$).

(3) Use $G_i^{\mathrm{C}l}$ and $G_i^{\mathrm{C}m}$ to calculate all bonding integrals at level two, i.e., $i \rightarrow k$ ($G_k^{\mathrm{C}i}$), $j \rightarrow k$ $G_k^{\mathrm{C}j}$).

(4) Use $G_k^{\mathrm{C}i}$ and $G_k^{\mathrm{C}j}$ to calculate all bonding integrals at level one, i.e., $k \rightarrow$ the root ($G_{\mathrm{root}}^{\mathrm{C}k}$).

(b) Search over children to calculate all parent-recursive functions $G_i^{\mathrm{P}}(\boldsymbol{r})$ [see Fig. 2(b2)]. The calculations were carried out from the root to every leaf level by level, which is the reverse of the traverse above. That is to say, we must calculate all the bonding connectivity integrals at level 1 first, and then calculate these at levels 2, 3, ..., up to level L. Therefore, the calculation procedures are as below.

(1) Calculate all bonding integrals at level one, i.e., the root $\rightarrow k$ (G_k^{F}).

(2) Use G_k^{F} to calculate all bonding integrals at level two, i.e., $k \rightarrow i$ (G_i^{F}), $k \rightarrow j$ (G_j^{F}).

(3) Use G_i^{F} and G_j^{F} to calculate all bonding integrals at level three, i.e., $i \rightarrow l$ (G_l^{F}), $i \rightarrow m$ (G_m^{F}).

(4) Use G_l^{F} and G_m^{F} to calculate all bonding integrals at level four, i.e., $l \rightarrow f$ (G_f^{F}), $l \rightarrow e$ (G_e^{F}), $m \rightarrow g$ (G_g^{F}), $m \rightarrow h$ (G_h^{F}).

It should be pointed out that Eq. (7) contains these items of $G_i^{\mathrm{C}\alpha}(\boldsymbol{r})$ [α=child(i)], which means that we must first calculate the child-recursive functions (a) and then the parent functions (b). By incorporating a bending potential into the bonding potential [18], this algorithm can also be extended to the DFT of semiflexible and rigid polyatomic fluids. Given that the bonding potential satisfies Eq. (4), this hierarchical algorithm is applicable not only to TPT1-based DFT, but also to TPT2-based DFT, GFD-based DFT, and many other versions of DFT. The difference between these versions of DFT is that they give different approximations of the excess free energy, and thus have no influence on the hierarchical algorithm. The TPT1 approach takes into account only the number of segmental connections and neglects the topology of polymers, which is included within the TPT2 approach. Therefore, in describing star or branched polymers, it would be more accurate to use TPT2 than TPT1. However, in order to illustrate our algorithm, we used the simple TPT1 approach in this work.

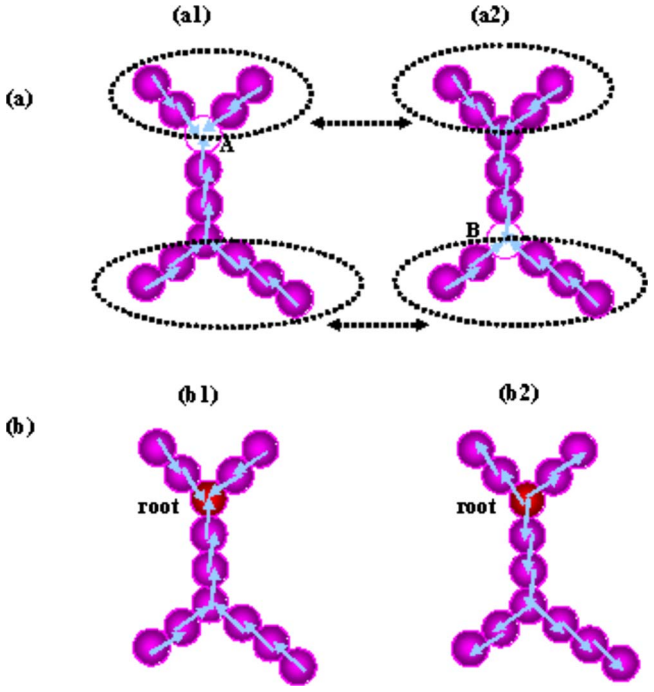

FIG. 3. (Color online) (a) Schematic diagrams for computing the local densities of segments A and B. The propagator functions inside the dashed circles are computed repeatedly. (b) Schematic diagrams for computing the local density using our algorithm in this work.

In other algorithms [6,7,27–29] where the segmental density was directly computed according to Eq. (6), the recursive functions for the polymers with complex architecture may be computed repeatedly. Figure 3 compares our algorithm with previous ones. In Fig. 3(a1), to calculate the segmental density of A, the recursive propagators from every leaf to segment A must be computed. These propagators may be repeatedly computed in getting another segmental density, for instance, of segment B [Fig. 3(a2)]. As is shown in Figs. 3(a1) and 3(a2), the propagators inside the dashed circles are repeatedly computed. To obtain all the segmental densities, we must record the propagators related to the articulated segment [for example, the segments A and B in Fig. 3(a)] in every calculation. The more articulated segments exist, the more propagators will be stored. This calculation is therefore more complicated. However, this problem of repeated computation does not appear in the case of linear chains, because there is no the articulated segment in a linear chain. On the contrary, in the case of complex chains, the propagators related to the articulated segments lead to a complicated computation. Our algorithm overcomes this problem by computing the propagator functions just on demand, i.e., every propagator function just needs to be computed one time, which greatly reduces the amount of calculation of DFT in the minimum limit. The idea of our algorithm is that we "fixed" a segment (the root) first, and computed all the child-recursive propagators [Fig. 3(b1)], and then obtained all the parent-recursive propagators [Fig. 3(b2)]. As illustrated above, these computations must be performed level by level, determined by the recursive relations of Eqs. (7) and (8).

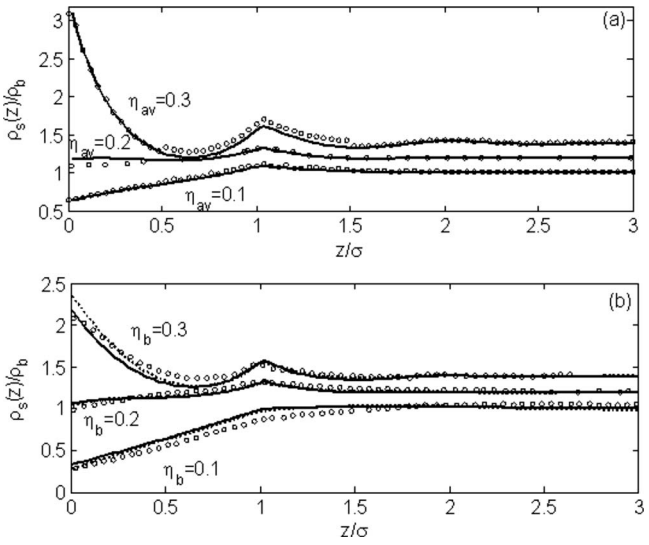

FIG. 4. (a) Segmental density profiles of linear 4-mers in a slit of 10σ at $\eta_{av}=0.1,0.3$ and 20-mers in a slit of 16σ at $\eta_{av}=0.2$. The average packing fraction in the slit pore is calculated from $\eta_{av}=(\pi/6)\rho_{av}\sigma^3=(\pi/6)\sigma^3(1/H)\int_0^H\rho_s(z)dz$. Circles represent simulation data from Yethiraj and Hall [31,32], and the solid line is from this work. The results for $\eta_{av}=0.2$ (0.3) are shifted upward by 0.2 (0.4). (b) Segmental density profiles of star polymers with three arms and five segments at each near a hard wall at $\eta_b=0.1,0.2,0.3$. Circles represent simulation data from Yethiraj and Hall [30], points denote DFT results from Malijevsky *et al.* [27], and solid line is the prediction from this work. The results for $\eta_b=0.2$ (0.3) are shifted upward by 0.2 (0.4).

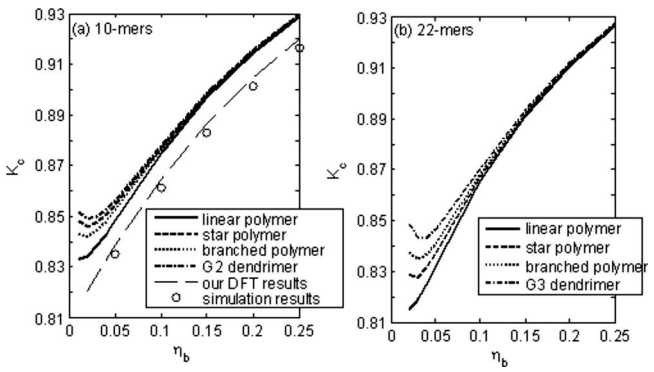

FIG. 5. Partitioning coefficients of hard-sphere chains of (a) 10-mers and (b) 22-mers in a slit of width $H=11\sigma$. (a) Open circles are simulation results of 4-mers in a slit of width $H=9\sigma$ from Yethiraj and Hall [31] The dashed line is the predictions in this work. The star polymer is comprised of three arms with two segments and one arm with three segments. The branched polymer is comprised of a backbone with four segments and two side chains with three segments in each. The G2 dendrimer is shown in Fig. 1(c), but with only two generations (ten segments). (b) Star polymer is comprised of three arms with five segments and one arm with six segments. The branched polymer is comprised of a backbone with seven segments and five side chains with three segments in each. The G3 dendrimer is shown in Fig. 1(c).

III. RESULTS AND DISCUSSION

To ensure that our approach does lead to a correct prediction, it would be ideal to test the density profiles of polymers for all architectures by comparison with Monte Carlo simulated data. Unfortunately, only data of linear and star polymers are available as a benchmark to validate this approach. We calculated the density profiles of linear and star polymers in a slit and show them in Figs. 4(a) and 4(b), where we also inserted the simulated data of Yethiraj and Hall [30] and DFT results of Malijevsky *et al.* [27] for comparison. For polymeric fluids confined in a slit, the density distribution varies only in the z direction, i.e., $\rho_{si}(\boldsymbol{r})=\rho_{si}(z)$, $G_i^{\mathrm{P}}(\boldsymbol{r})=G_i^{\mathrm{P}}(z)$, and $G_i^{\mathrm{C}\alpha}(\boldsymbol{r})=G_i^{\mathrm{C}\alpha}(z)$ $[\alpha=\mathrm{child}(i)]$.

Obviously, for both linear and star polymers at various packing fractions, all our calculation results are in good agreement with the MC data and with the DFT results from Malijevsky *et al.* [27]. The difference between our results and the DFT data from Malijevsky *et al.* occurs only within the region near the wall at high packing fractions. The contact value of our calculation at $\eta_b=0.3$ is much closer to the MC data than the results from Malijevsky *et al.*. In the DFT of Malijevsky *et al.*, the segmental density is directly calculated by Eq. (6). The disadvantage of this calculation is that the recursive functions, which are a multiple multiplication of the other propagators, have to be repeatedly computed. This repeated calculation of multiple multiplications may lead to a slight deviation of the numerical solution. As discussed above, our algorithm avoids this deviation by computing the propagator function just on demand.

To consider the effect of the architecture on the microstructure and behavior of polymers, we further investigated the partitioning coefficient of polymers of different architectures in a slit of $H=11\sigma$. The partitioning coefficient describes the division of the polymer chain in the slit and bulk phases, and is generally defined as $K_c=\rho_{av}/\rho_b$, where $\rho_{av}=(1/H)\int_0^H\rho_s(z)dz$ is the average segmental density of polymer chains in the slit. Figures 5(a) and 5(b) show the partitioning coefficients of 10-mers and 22-mers with different architectures in the slit of $H=11\sigma$, respectively. In Fig. 5(a), we also compare our calculation results for 4-mers in a slit of $H=9\sigma$ to the MC data in the same conditions from Yethiraj and Hall [31]. It is found that our predictions agree well quantitatively with the MC data. The difference in the packing fractions of polymer chains in the slit and the bulk phases is due to the depletion effect, because the walls of the slit do not have any attraction for the segments. As a result, in the range of packing fractions from 0 to 0.25, the average density of polymer chains in the slit is always smaller than the bulk density, not only for the 10-mers but also for the 22-mers. However, the different architectures exhibit different behaviors in the partitioning coefficient, especially for the case of 22-mers as shown in Fig. 5(b). Interestingly, the partitioning coefficients of branched, star, and G3 dendritic polymers of 22-mers decrease to a minimum at extremely low packing fractions, and then increase monotonically with packing fraction. Moreover, the partitioning coefficients of branched, star, and G3 dendritic polymers of 22-mers are always larger than that of the linear polymer of 22-mers. That is to say, it is more difficult for linear polymer of 22-mers than for other architecture polymers to enter the slit,

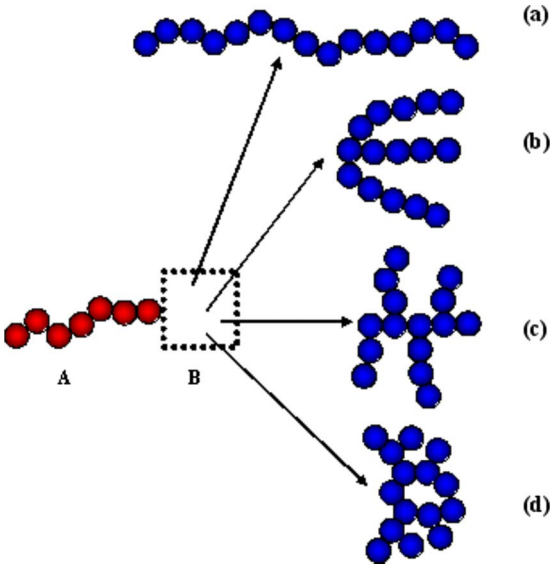

FIG. 6. (Color online) Schematic diagrams of diblock copolymers of 22-mers with (a) linear, (b) star, (c) branched, and (d) dendritic tails. The hydrophilic head (denoted by A) is comprised of seven segments, and the hydrophobic tail (denoted by B) is comprises of 15 segments.

which may be because the linear polymer possesses a long-chain architecture while the star, branched, and dendritic polymers possess spherelike architecture.

To further explore the practical application of the proposed algorithm, we also investigate the self-assembly of diblock copolymers. The diblock copolymer comprises a simple linear head (represented as A) and a tail with complex architecture (represented as B), such as linear, star, branched, and dendritic structures. The former represents the hydrophilic segments, and the latter represents the hydrophobic segments. A schematic diagram is shown in Fig. 6. The intermolecular pair potential of segments is represented by a square well potential, given by

$$\varphi_{ij}(r) = \begin{cases} \infty, & r < \sigma, \\ \varepsilon_{ij}, & \sigma \leqslant r \leqslant \gamma\sigma, \\ 0, & r > \gamma\sigma, \end{cases} \tag{9}$$

where $i,j=A$ or B, r is the distance between two segments, $\gamma\sigma$ is the square well width, and ε_{ij} is the energy parameter. In this work, the attractive width is fixed at $\gamma=1.2$. The pair interaction between like segments (AA or BB) is always attractive and that between unlike segments is always repulsive. The unlike-pair interaction is fixed at $\varepsilon_{AB}=0.5k_BT$. In order to mimic the hydrophobic effect, we assume that the attraction between BB segments ($\varepsilon_{BB}=-1.5k_BT$) is stronger than that between AA segments ($\varepsilon_{AA}=-0.5k_BT$), where the negative stands for attraction, k_B is the Boltzmann constant, and T is the absolute temperature.

Figure 7 shows the average packing fractions of diblock copolymers in a slit of $H=14\sigma$. All curves present an abrupt jump. The first abrupt jump located at $\eta_b=0.021$ (linear tail), 0.031 (star tail), 0.035 (branched tail), and 0.041 (dendritic tail). These abrupt jumps correspond to the phase transition

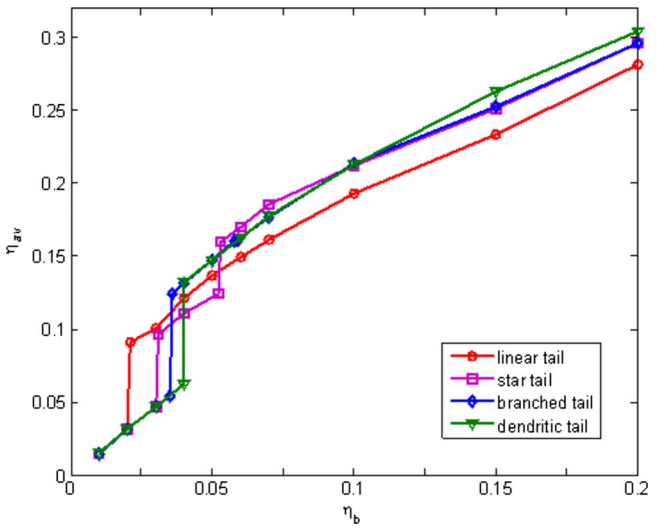

FIG. 7. (Color online) Average packing fraction of diblock copolymers in a slit of $H=14\sigma$.

from a disordered state to an ordered phase. The bulk packing fraction corresponding to the jump increases with the complexity of the molecular architecture. A complex architecture elevates the driving force of molecular self-assembly because it loses more configurational entropy than a simple architecture. Thus, the copolymers with tails with complex architecture need a higher bulk packing fraction as a driving force on molecular self-assembly. Interestingly, the second jump occurs at $\eta_b=0.053$ for the copolymers with star tails. To get further insight into the microscopic behavior of copolymers before and after the phase transition, we present the local density profiles of A and B segments at different bulk packing fractions in Figs. 8 and 9. Since the curve corresponding to the star tail exhibits two abrupt jumps, the local

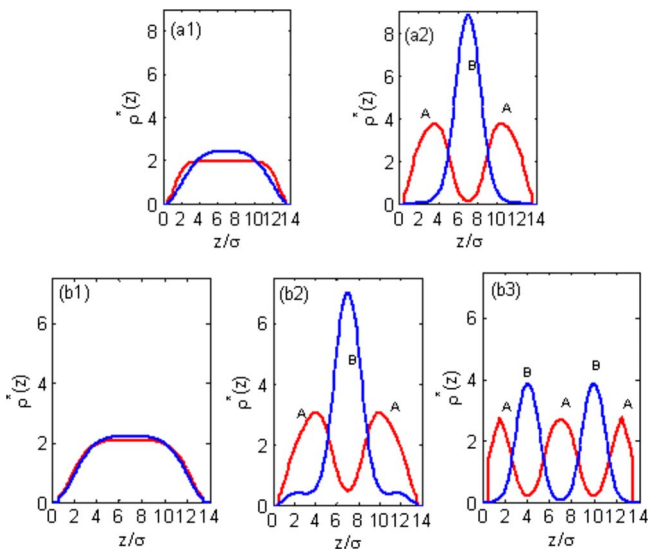

FIG. 8. (Color online) Segmental density profiles (red lines for A segment and blue lines for B segment) of diblock copolymers with (a) linear and (b) star tails in a slit of width $H=14\sigma$. The bulk packing fractions are η_b=(a1) 0.020, (a2) 0.021, (b1) 0.030, (b2) 0.031, and (b3) 0.053.

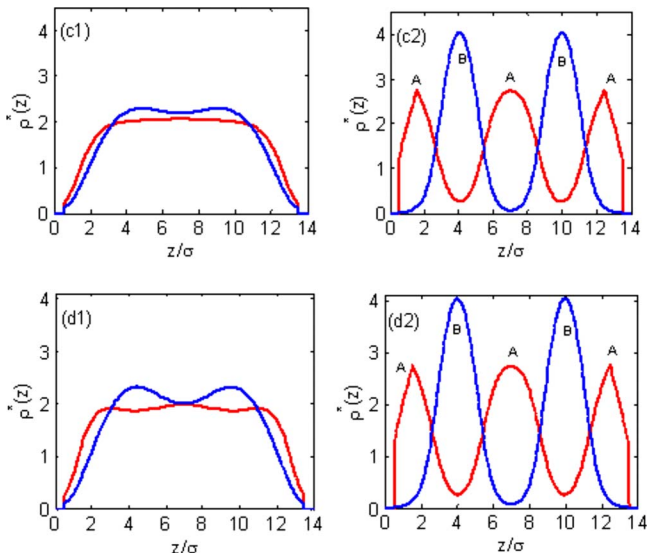

FIG. 9. (Color online) Segmental density profiles (red lines for *A* segment and blue lines for *B* segment) of diblock copolymers with (c) branched and (d) dendritic tails in a slit of width $H=14\sigma$. The bulk packing fractions are η_b=(c1) 0.035, (c2) 0.036, (d1) 0.041, and (d2) 0.042.

structures of the copolymers at three bulk packing fractions are presented in Fig. 8. For the copolymer with linear tail [see Fig. 8(a)], the density profile at $\eta_b=0.020$ shows a disordered state of the confined diblock copolymer, while it exhibits an *ABA* trilayer film structure at $\eta_b=0.021$. Interestingly, for the copolymer with star tail, besides the phase transition from a disordered state to the trilayer film structure, the copolymer also presents a structural evolution from the *ABA* trilayer film structure to an *ABABA* five-layer film structure. The structure evolution just happens at the second jump, i.e., bulk packing faction $\eta_b=0.053$. That is to say, the structure evolution probably leads to the second abrupt jump in the curve corresponding to the star tail in Fig. 7. In particular, Fig. 9 shows that copolymers with branched and dendritic tails self-assembled into the five-layer film structure directly, without the existence of a trilayer structure, which implies that the trilayer film structure is not stable in the case studied. As discussed above, the copolymers with complex architecture tails possess spherelike structures, with a smaller radius of gyration than that of a simple linear architecture. The resulting thickness of the periodicity of the self-assembled lamellae is also smaller than that of the linear polymer. Thus, the copolymers with complex architectures self-assemble into a five-layer structure, while the linear copolymer self-assembles into a trilayer structure. More ordered layers would be assembled, if the width of the slit was large enough [26].

IV. CONCLUSIONS

In summary, by introducing a tree-type representation for polymers, we proposed a universal version of density-functional theory for inhomogeneous polymers with complex architecture. The DFT version is applicable to polymers of different architectures, including linear, star, branched, and dendritic structures. Though these formulations were derived in the case of a slit, our algorithm calculating the complex chain connectivity is suitable for the bulk or other confined phases. The algorithm should extend greatly the investigations of physical properties of polymers with complex architectures.

A good agreement of the calculation results by our approach and the available MC data confirms the validity of the algorithm. By using the proposed approach, we calculated the partitioning coefficients of polymers of different architectures in a slit, and found that the partitioning coefficients of branched, star, and G3 dendritic polymers of 22-mers decrease to a minimum at extremely low packing fraction, and then increase monotonically with packing fraction. Moreover, based on the partitioning coefficients, it is found that it is more difficult for the linear polymer of 22-mers to enter the slit than for the branched, star, and dendritic polymers.

In addition, we also investigated the self-assembly of diblock copolymers with different tails in the slit. It is found that the linear copolymer self-assembled into a trilayer film structure, while the copolymers with branched and dendritic tails self-assembled into a five-layer film structure. Interestingly, the copolymer with star tail self-assembled into a trilayer film structure first, and the trilayer film structure evolved into a five-layer film structure with increase of the bulk packing fraction. Moreover, it is found that the bulk packing fractions, corresponding to the phase transition from a disordered state to an ordered state, increase with the complexity of the tail architecture, because complex architecture, say, a dendrimer, elevates the driving force of molecular self-assembly, and the copolymers with tails with complex architecture lose more configurational entropy than a simple linear copolymer.

ACKNOWLEDGMENTS

This work was supported by the National Natural Science Foundation of China (Grant Nos. 20776005, 20736002, and 20874005), Beijing Novel Program (Grant No. 2006B17), the Program for New Century Excellent Talents (Grant No. NCET-06-0095) from the Ministry of Education, and the "Chemical Grid Project" and Excellent Talents Funding of BUCT. X.X. is grateful to Dr. Bryk for providing the MC data of star polymers, and also grateful to Lisheng Cheng for providing important and helpful discussion about this work.

[1] D. Chandler, J. D. McCoy, and S. J. Singer, J. Chem. Phys. **85**, 5971 (1986).
[2] E. Kierlik and M. L. Rosinberg, J. Chem. Phys. **97**, 9222 (1992).
[3] C. E. Woodward and A. Yethiraj, J. Chem. Phys. **100**, 3181 (1994).
[4] C. E. Woodward and J. Forsman, Macromolecules **37**, 7034 (2004).
[5] Y. Rosenfeld, Phys. Rev. Lett. **63**, 980 (1989).
[6] R. Roth *et al.*, J. Phys.: Condens. Matter **14**, 12063 (2002).
[7] Y. X. Yu and J. Z. Wu, J. Chem. Phys. **117**, 2368 (2002).
[8] G. A. Mansoori, N. F. Carnahan, K. E. Starling, and T. W. Leland, Jr., J. Chem. Phys. **54**, 1523 (1971).
[9] P. Bryk, O. Pizio, and S. Sokolowski, J. Chem. Phys. **122**, 194904 (2005).
[10] P. Bryk and S. Sokolowski, J. Chem. Phys. **121**, 11314 (2004).
[11] P. Bryk *et al.*, J. Phys. Chem. B **109**, 2977 (2005).
[12] D. P. Cao, M. H. Zhu, and W. C. Wang, J. Phys. Chem. B **110**, 21882 (2006).
[13] D. P. Cao and J. Z. Wu, Macromolecules **38**, 971 (2005).
[14] D. P. Cao, T. Jiang, and J. Z. Wu, J. Chem. Phys. **124**, 164904 (2006).
[15] D. P. Cao and J. Z. Wu, Langmuir **21**, 9786 (2005).
[16] D. P. Cao and J. Z. Wu, Langmuir **22**, 2712 (2006).
[17] Z. D. Li, J. Z. Wu, and Z.-G. Wang, Biophys. J. **94**, 737 (2008).
[18] D. P. Cao and J. Z. Wu, J. Chem. Phys. **121**, 4210 (2004).
[19] T. Jiang, Z. D. Li, and J. Z. Wu, Macromolecules **40**, 334 (2007).
[20] X. F. Xu, D. P. Cao, and W. C. Wang, J. Phys.: Condens. Matter **20**, 425221 (2008).
[21] D. P. Cao, L. S. Cheng, and W. C. Wang, Chin. Phys. **16**, 2296 (2007).
[22] S. Sen *et al.*, J. Chem. Phys. **101**, 9010 (1994).
[23] A. Yethiraj and C. E. Woodward, J. Chem. Phys. **102**, 5499 (1995).
[24] C. E. Woodward, J. Chem. Phys. **94**, 3183 (1991).
[25] A. Yethiraj, J. Chem. Phys. **109**, 3269 (1998).
[26] L. S. Cheng and D. P. Cao, J. Phys. Chem. B **111**, 10775 (2007).
[27] A. Malijevsky, P. Bryk, and S. Sokolowski, Phys. Rev. E **72**, 032801 (2005).
[28] S. Tripathi and W. G. Chapman, J. Chem. Phys. **122**, 094506 (2005).
[29] E. Kierlik and M. L. Rosinberg, J. Chem. Phys. **100**, 1716 (1994).
[30] A. Yethiraj and C. K. Hall, J. Chem. Phys. **94**, 3943 (1991).
[31] A. Yethiraj and C. K. Hall, Macromolecules **23**, 1865 (1990).
[32] A. Yethiraj and C. K. Hall, Mol. Phys. **73**, 503 (1991).